

Hubble tension tomography: BAO vs SnIa distance tension

Dimitrios Bousis^{1,*} and Leandros Perivolaropoulos^{1,†}

¹*Department of Physics, University of Ioannina, GR-45110, Ioannina, Greece*

(Dated: May 21, 2024)

We investigate the redshift dependence of the Hubble tension by comparing the luminosity distances obtained using an up-to-date BAO dataset (including the latest DESI data) calibrated with the CMB-inferred sound horizon, and the Pantheon+ SnIa distances calibrated with Cepheids. Using a redshift tomography method, we find: 1) The BAO-inferred distances are discrepant with the Pantheon+ SnIa distances across all redshift bins considered, with the discrepancy level varying with redshift. 2) The distance discrepancy is more pronounced at lower redshifts ($z \in [0.1, 0.8]$) compared to higher redshifts ($z \in [0.8, 2.3]$). The consistency of Λ CDM best fit parameters obtained in high and low redshift bins of both BAO and SnIa samples is investigated and we confirm that the tension reduces at high redshifts. Also a mild tension between the redshift bins is identified at higher redshifts for both the BAO and Pantheon+ data with respect to the best fit value of H_0 in agreement with previous studies which find hints for an 'evolution' of H_0 in the context of Λ CDM. These results confirm that the low redshift BAO and SnIa distances can only become consistent through a re-evaluation of the distance calibration methods. An $H(z)$ expansion rate deformation alone is insufficient to resolve the tension. Our findings also hint at a possible deviation of the expansion rate from the Planck18/ Λ CDM model at high redshifts $z \gtrsim 2$. We show that such a deformation is well described by a high redshift transition of $H(z)$ like the one expressed by Λ_s CDM even though this alone cannot fully resolve the Hubble tension due to its tension with intermediate/low z BAO data.

I. INTRODUCTION

The sound horizon scale r_s at recombination (standard ruler) and the standardized bolometric absolute magnitude M_B of Type Ia supernovae (SnIa standard candles) have been used as probes for the measurement of cosmological distances and thus for the measurement of the Hubble constant H_0 , the most fundamental parameter of cosmology. The best fit values of H_0 obtained using the two distance calibrators are at 5σ discrepancy with each other. This is the most important challenge[1–3] for the current standard cosmological model the Λ CDM.

Each type of measurement makes specific assumptions whose possible violation would lead to significant systematic errors that would invalidate the accuracy of the corresponding measurement. Measurements based on SnIa standard candles assume the validity of the distance ladder approach and in particular that physical laws and environmental effects around calibrated SnIa are the same in all the three rungs of the distance ladder. Measurements based on the sound horizon scale used as a standard ruler assume that the physical laws before recombination are consistent with the standard cosmological model and that the expansion history of the universe $H(z)$ is consistent with the standard Λ CDM model and its parameters determined by the Planck18[4]

(Planck18/ Λ CDM).

In accordance with the above three types of assumptions there are three classes of models for the resolution of the Hubble tension:

- **Ultralate time models:** These models[5–7] assume that there is a physics or environmental change between the second and third rungs of the distance ladder ie that the Cepheid calibrated SnIa are not the same as the Hubble flow SnIa either due to a change of the physical laws or due to some change in their structure or environment (dust, metalicity etc). Thus, M_B in the third rung of the distance ladder (Hubble flow rung $z \in [0.01, 0.1]$) is lower than the value measured in the second rang. Thus these models explore the degeneracy between H_0 and M_B in the context of the Hubble flow observable

$$\mathcal{M} \equiv M_B + 5 \log \frac{c/H_0}{Mpc} + 25 \quad (1.1)$$

to lead to a lower H_0 measurement in the context of the distance ladder measurements.

The main problem of this class of models is fine tuning. There is no current clear theoretical motivation for the assumed physics transition at such ultralate redshifts ($z \sim 0.01$) even though it is straightforward to construct such models using a degree of fine tuning[8]. On the other hand, the physics transitions hypothesis is easily testable using a wide redshift data and

* dimitriosbousis2002@gmail.com

† leandros@uoi.gr

in fact there are some hints for such an affect in both Cepheid and Tully-Fisser data [9, 10].

- **Early time models:** These models assume physics beyond the standard model to decrease the sound horizon scale at recombination

$$r_s = \int_{z_{rec}}^{\infty} \frac{dz c_s(z)}{H(z; \Omega_{0b} h^2, \Omega_{0\gamma} h^2, \Omega_{0CDM} h^2)} \quad (1.2)$$

to a lower value induced by Early Dark Energy [11–17] (EDE), modified gravity[18–27] or dark radiation[28–30]. Thus, these models exploit the degeneracy of r_s with H_0 in the context of the observable angular scale of the CMB sound horizon r_s

$$\theta_s = \frac{r_s H_0}{\int_0^{z_{rec}} 1/E(z)} \quad (1.3)$$

to lead to a higher value of H_0 while respecting the best fit Planck18/ Λ CDM form of $E(z) \equiv H(z)/H_0$ between recombination and present time.

The main problem of this class is that despite fine tuning of theoretical models that support them, they are only able to decrease the statistical significance of the Hubble tension and they can not fully eliminate it. In addition, they favor a higher value of matter density parameter Ω_{0m} thus worsening the S_8 tension [31–34].

- **Late time models ($H(z)$ deformation):** These models assume that there is deformation of the Hubble expansion history $H(z)$ with respect to the Planck18/ Λ CDM prediction at late cosmological times ($z \lesssim 2$) [35–42]. This deformation shifts the value of H_0 measured by the sound horizon scale standard ruler to a value consistent with the distance ladder measurement by effectively changing the denominator of eq. (1.3). However, as discussed in the present analysis even this model has difficulty to fit simultaneously BAO and SnIa data.

The main problem of this class of models is that $E(z) \equiv H(z)/H_0$ deformations are highly constrained by BAO and SnIa data in redshifts larger than $z \simeq 0.1$ [31, 39, 41, 43–54]. Thus, this class of models have been put in disfavor during the last few years. Exception constitutes the Λ_s CDM model which shifts the deformation to high redshifts ($z \simeq 2$) and makes it abrupt so that it has a minimal effect on late data while maintaining consistency with the distance to the CMB sound horizon at last scattering [55].

The $H(z)$ deformation models are designed to be consistent with three types of cosmological data.

- Low z ($z \lesssim 0.1$) calibrated Hubble flow data (eg the SH0ES data [56]) which measure $H_0 = 73.04 \pm 1 \text{ km/secMpc}^{-1}$.
- The distance to the CMB sound horizon scale r_s as measured by the Planck CMB power spectrum.
- The distance to BAO and SnIa data as obtained with the corresponding calibrators (CMB r_s for BAO and Cepheid M_B for SnIa).

These models perform very well in fulfilling the first two requirements. However, they all have problems fulfilling the third requirement. An interesting questing thus emerges

Is this difficulty due to the fact that there is a specific feature missed by the $H(z)$ parametrizations considered so far? Or there is a generic inconsistency between the BAO and SnIa data when the proper calibration is used in each case?.

This question is addressed in the present analysis using a redshift tomography method. We thus test the consistency of the cosmological distances obtained with the properly calibrated BAO and SnIa data with each other and with the Planck18/ Λ CDM $E(z)$ in various redshift bins. We thus identify those redshifts where the distances obtained with the two classes of data are consistent and search for redshifts where there is a generic inconsistency between these distances. For the later redshift range it would be impossible to fit simultaneously the BAO and SnIa for any parametrization $H(z)$ due to the generic inconsistency between the two classes of data.

We thus find the level of inconsistency between r_s calibrated BAO distances and Cepheid M_B calibrated SnIa measured distances as a function of redshift. This may be interpreted as *the level of the Hubble tension as a function of redshift*. We also find the level of consistency of the measured distances with the predictions of Planck18/ Λ CDM as a function of redshift.

Recent studies have investigated the redshift dependence of the Hubble tension using various probes and methods [57–62]. These analyses consistently find a reduction in the tension at higher redshifts, hinting at a possible low-redshift origin for the discrepancy. However, the specific redshift range and significance of this effect varies between studies, motivating further investigation.

Previous studies [63] have demonstrated a general trend for inconsistency between the cosmological distances obtained with BAO and SnIa data. We quantify this finding using redshift tomography and

a more extensive up-to-date BAO dataset. Promising approaches like Λ_s CDM [55, 64] are also investigated, which introduce a rapid transition in $H(z)$ at high redshifts to improve consistency with SnIa data. However, we find that the fundamental tension between BAO and SnIa data creates problems even for these models.

Potential systematic effects that could influence the redshift dependence of the Hubble tension are an important consideration. For example, selection effects in the SnIa samples at different redshifts [65] or evolution in the SnIa luminosity with redshift [66] could impact the tension measurement. On the BAO side, the determination of the sound horizon scale r_d relies on assumptions about early universe physics that could potentially be violated [67]. While a full investigation of these effects is beyond the scope of this paper, they are important caveats to keep in mind when interpreting the results.

The structure of this paper is the following: In section II we present the method used in our analysis which involves binning distance measurements using BAO data and comparing them with the corresponding distances obtained with binned Pantheon+ SnIa data. This tomography is used for estimating the statistical level of the calibrator mismatch as a function of redshift (Hubble tension tomography). Our results are presented in section III. Finally, section IV we conclude, summarize and discuss possible extensions of our analysis.

II. METHOD: BINNING DISTANCE MEASUREMENTS WITH PANTHEON+ AND BAO

The Pantheon+ sample provides SnIa luminosity distance d_L and distance moduli μ measurements for redshifts in the range $z \in [0.001, 2.3]$. These measurements are calibrated by the second rung of the distance ladder using Cepheids measuring the SnIa absolute magnitude as $M_B = -19.25 \pm 0.01$ [9, 56, 68].

Assuming validity of the distance duality relation $d_L = (1+z)^2 D_A$, the BAO data calibrated by the comoving CMB sound horizon scale standard ruler $r_d = 147.1 Mpc$ at the end of the baryonic drag epoch [4], also lead to measurements of the luminosity distance d_L and distance moduli μ , in the redshift range $z \in [0.1, 2.4]$. The CMB-inferred sound horizon scale r_d is determined by fitting the standard Λ CDM model to the Planck CMB power spectra data, assuming standard pre-recombination physics [4]. It corresponds to the comoving size of the sound horizon at the end of the baryonic drag epoch, when photon pressure no longer supports acoustic oscil-

lations in the primordial plasma (see [69] for a review). The consistency level of these measurements with the corresponding measurements of the Pantheon+ sample as a function of redshift bins reflects the level of the Hubble tension in redshift space. The method to perform this Hubble tension tomography is described in this section.

II.1. Binning the distance moduli residual of Pantheon+

The Pantheon+ sample [70, 71] consists of a table of 1701 rows (plus a header) and 47 columns. A 1701×1701 covariance matrix is part of it and it represents the covariance between all the SnIa due to systematic and statistical uncertainties of the distance moduli. In this analysis the information we need to utilize from the sample is:

- The Hubble diagram redshift (with CMB and peculiar velocity corrections)
- The corrected apparent magnitude of the SnIa as well as its uncertainty which includes errors due to peculiar velocity
- The distance moduli μ calculated by subtracting the absolute magnitude of the SnIa $M_{SHOES} = -19.253$ from the apparent magnitude and also their uncertainties obtained through the diagonal of the covariance matrix
- The distance moduli μ_{Ceph} , as found by the SHOES distance ladder analysis, of the SnIa in Cepheid hosts with their uncertainties being incorporated in the covariance matrix

The data can be found in the github repository [in this url](#).

The SnIa distance moduli of the Pantheon+ sample measured in the Hubble flow are used to constrain the luminosity distance d_L through the relation

$$\mu(z) = m(z) - M_B = 5 \log(d_L(z)/Mpc) + 25 \quad (2.1)$$

where the luminosity distance is connected with the Hubble expansion rate:

$$d_L(z) = (1+z)c \int_0^z \frac{dz'}{H_0 E(z')} \quad (2.2)$$

c is the speed of light and the dimensionless Hubble parameter E in the context of Λ CDM is given by:

$$E = \sqrt{(a^{-3}\Omega_{0m} \left(1 + \frac{a_{eq}}{a}\right) + (1 - \Omega_{0m}(1 + a_{eq}))} \quad (2.3)$$

with a_{eq} the scale factor corresponding to the time when matter and radiation were equal

$$a_{eq} = \frac{1}{(z_{eq} + 1)}, z_{eq} = 2.5 \cdot 10^4 \Omega_{0m} h^2 (T_{CMB}/2.7)^{-4} \quad (2.4)$$

with $T_{CMB} = 2.7255K$.

To get the theoretical distance modulus corresponding to the Planck18/ Λ CDM model we simply need to incorporate the Planck 2018 values for the present matter density parameter $\Omega_{0m} = 0.3166$ and the Hubble constant $H_0 = 67.4 \text{ km s}^{-1} \text{ Mpc}^{-1}$ ($h = 0.674$) into equations (2.1)-(2.3) to obtain $\mu_{P\Lambda CDM}(z)$.

We define the distance modulus residual between the theoretical values of the Planck18/ Λ CDM model and the observational data obtained through the Pantheon+ sample:

$$\Delta\mu(z_i) \equiv \mu_{obs}(z_i) - \mu_{P\Lambda CDM}(z_i) \quad (2.5)$$

We have binned this residual in 13 evenly spaced bins for $z \in [0.001, 2.3]$ to compare with corresponding BAO data. The redshift for each bin is the mean of all redshifts within said bin. For the calculation of the distance modulus for each bin the covariance matrix was incorporated. This was done by first constructing a vector for each bin j with components

$$Q_i = \Delta\mu(z_i) - \mu_{cj} \quad (2.6)$$

Components of Q out of the j bin were set to 0. In (2.6), μ_{cj} is the residual distance modulus in the j^{th} bin and $\Delta\mu(z_i)$ is defined by eq. (2.5) for a given redshift z_i in the redshift range of the corresponding bin. Then to obtain the best fit value of $\Delta\mu(z_{Meanj})$ (with z_{Meanj} being the mean redshift in the redshift range of the j^{th} bin), we found the value of the best fit j^{th} bin distance modulus residual μ_{cj} that minimizes the appropriate χ^2 function:

$$\chi_j^2 = Q^T \cdot C^{-1} \cdot Q \quad (2.7)$$

where C^{-1} is the inverse of the covariance matrix of the Pantheon+ sample. Using the definition (2.6) in (2.7) the proper part of the inverse covariance matrix corresponding to the j^{th} bin is automatically selected. In this fashion we end up with 13 different Planck18/ Λ CDM residual distance moduli values μ_{cj} , one for each bin. The uncertainties for each bin j were calculated in the standard way using the inverse of the Fisher matrix

$$F = \frac{1}{2} \frac{\partial^2 \chi^2(\mu_{cj})}{\partial \mu_{cj}^2} \quad (2.8)$$

We have also split the Pantheon+ sample into two larger bins for redshifts $0.1 < z < 0.8$ and $0.8 < z <$

2.3 in order to fit for each bin the Λ CDM cosmological parameters and identify the self consistency of the Pantheon+ sample and also compare with the corresponding best fit parameters of a BAO sample discussed in the next subsection. For each bin a data vector can be constructed as follows:

$$Q'_i = \begin{cases} m_{B,i} - M_B - \mu_i^{Ceph} & , \text{Cepheid hosts} \\ m_{B,i} - M_B - \mu_{\Lambda CDM}(z_i) & , \text{Otherwise} \end{cases} \quad (2.9)$$

where in each bin we have also included the Cepheid host SnIa distance moduli as found by the SH0ES distance ladder analysis. For each bin we evaluate the χ^2 function:

$$\chi_{bin}^{\prime 2} = Q^{\prime T} \cdot C^{-1} \cdot Q' \quad (2.10)$$

and minimize it to obtain the best fit values for M_B , Ω_{0m} and h and the corresponding likelihood contours discussed in the next section. We have also constructed the distance moduli residual for the two new large bins as described above for the smaller bins. These distance moduli residuals and Λ CDM parameter contours were then compared with the corresponding BAO quantities described in the next subsection.

II.2. Distance moduli from BAO

We have compiled a list of transverse BAO measurements, of the rescaled comoving angular diameter distance $\frac{D_M}{r_d}$, where r_d is the sound horizon scale during the drag epoch in which the photon drag on regular matter (baryons) becomes negligible. The sample created includes both data as recent as the DESI 2024 [72] as well as some earlier measurements including the latest releases of the Sloan Digital Sky Survey (SDSS) and the Dark Energy Survey (DES). The full sample we use is shown in Table I

The data in Table I are from anisotropic BAO analyses, they have been derived using a fiducial model to convert the observed data into physical distances, and then isolating the angular component (D_M) to compute D_M/r_d . The distinction between anisotropic BAO analyses and 2D BAO data may be described as follows:

- Anisotropic BAO analyses incorporate the full three-dimensional distribution of galaxies. These analyses take into account both the radial and transverse components simultaneously, often using a fiducial cosmological model to convert observed angles and redshifts into physical distances. This allows for a more detailed understanding of the BAO signal and its anisotropies, but it introduces model dependencies in the process.

- In 2D BAO analyses, the BAO signal is examined in a two-dimensional plane, often focusing separately on the transverse (angular) and radial (line-of-sight) directions. This method typically avoids using a fiducial cosmological model to convert angular separations and redshifts directly into physical distances. Instead, it keeps the analysis in observational units (angles and redshifts), which can then be used to infer cosmological parameters in a somewhat model-independent way. This approach is designed to minimize assumptions about the underlying cosmology when extracting the BAO signal.

The distance modulus residual can now be written as:

$$\begin{aligned}\Delta\mu(z_i) &= \mu_{obs}(z_i) - \mu_{PACDM}(z_i) \\ &= 5\log\left(\frac{d_L^{obs}(z_i)}{d_L^{PACDM}(z_i)}\right)\end{aligned}\quad (2.11)$$

The ratio of the observed luminosity distance over the Planck 2018 theoretical luminosity distance, $\frac{d_L^{obs}(z_i)}{d_L^{PACDM}(z_i)}$, can be replaced by:

$$\frac{d_L^{obs}(z_i)}{d_L^{PACDM}(z_i)} = \frac{D_M^{obs}(z_i)}{D_M^{PACDM}(z_i)}\quad (2.12)$$

since the comoving angular distance D_M is simply $D_M = (1+z)D_A$, where D_A is the angular diameter distance which in turn is $D_A = d_L/(z+1)^2$. Therefore, the distance moduli residuals can be written as:

$$\Delta\mu(z_i) = 5\log\left(\frac{D_M^{obs}(z_i)}{D_M^{PACDM}(z_i)}\right)\quad (2.13)$$

where we have estimated $D_M^{obs}(z_i)$ by multiplying the entries of Table I by the best fit value $r_d = 147.18 Mpc$ from Planck18[4]. For the theoretical Planck18/ Λ CDM $D_M(z_i)$ we have incorporated the Planck 2018 Λ CDM values for the Hubble constant and the present matter density parameter as mentioned above in section II.1. We also assume flat universe and thus use the present Λ density parameter $\Omega_{0\Lambda} = 0.685$, the present radiation density parameter $\Omega_{0r} = 9.26 * 10^{-5}$ and the sound horizon drag scale $r_d = 147.18$:

$$D_M^{PACDM}(z_i) = \int_0^{z_i} \frac{c}{H_0 \sqrt{\Omega_{0m}(1+z)^3 + \Omega_{0\Lambda} + \Omega_{0r}(1+z)^4}} dz\quad (2.14)$$

The distance modulus residual $\Delta\mu(z_i)$ can then be plotted as a function of redshift z_i (left panel of Fig.

1). The uncertainties are calculated using the error propagation method as follows:

$$\sigma_i = \frac{5}{\ln 10} \frac{1}{D_M^{obs}(z_i)} \cdot \sigma_{D_M^{obs}(z_i)}\quad (2.15)$$

where we have omitted the effect of the uncertainty of r_d because it is easy to show that it is subdominant. We have also merged some of the points which have the same effective redshift value. This was done by first calculating the weighted D_M ratios [90]:

$$D_{M,weighted} = \frac{\sum D_{Mi}/\sigma_i}{\sum 1/\sigma_i}\quad (2.16)$$

and then calculating the combined uncertainty:

$$\sigma_{combined} = \frac{1}{\sqrt{\sum 1/\sigma_i^2}}\quad (2.17)$$

For the construction of the right panel of Fig. 1, we have also considered three redshift bins for redshift ranges $0.1 < z < 0.8$, $0.8 < z < 2.0$ and $2.0 < z < 2.5$. For each bin we get the distance modulus residuals $\Delta\mu_i$ as shown in Eq. (2.11) and the uncertainties σ_i for each residual (see Eq. 2.15). The redshift for each bin is the mean of all the redshifts of said bin, the distance modulus residual is the weighted mean:

$$\Delta\mu_{bin} = \frac{\sum \frac{\Delta\mu_i}{\sigma_i^2}}{\sum 1/\sigma_i^2}\quad (2.18)$$

and the uncertainty is the combined uncertainty:

$$\sigma_{bin} = \sqrt{\frac{1}{\sum 1/\sigma_i^2}}\quad (2.19)$$

The bin residual distance moduli are shown in the right panel of Fig. 1 along with the two Pantheon+ bins discussed at the end of section II.1 for a comparison to be made. The comparison is discussed in the next section.

For the comparison of the best fit cosmological parameters h and Ω_{0m} with Pantheon+, we have constructed two redshift bins in the same redshift ranges as those used for the Pantheon+ data ($0.1 < z < 0.8$ and $0.8 < z < 2.5$)¹.

Thus, for each bin we construct the χ^2 function as follows:

$$\chi^2 = \sum \frac{(D_M^{obs}(z_i) - D_M^{ACDM}(z_i))^2}{\sigma_{D_M^{obs}(z_i)}^2 + \sigma_{r_d}^2}\quad (2.20)$$

¹ It should be noted here that the redshift range of the second bin goes beyond redshift 2.3, up to redshift 2.5 since we have BAO data for these redshifts as well.

TABLE I: D_M/r_d measurements and the corresponding references. The sample consists of 33 measurements. Measurements with an asterisk are the D_M/r_d value calculated using the angular diameter distance $D_A = D_M/(1+z)$ and the fiducial r_d^{fid} value $r_d = 147.18 Mpc$ obtained by Planck18 in the context of Λ CDM. More details about the construction of the * datapoints are presented in the Appendix. V.

N	z_{eff}	D_m/r_d	References	Year
1	0.32*	8.54±0.25	Chuang et al [73]	2016
2	0.32	8.76±0.14	BOSS collaboration [74]	2016
3	0.38	10.27±0.15	BOSS collaboration [74]	2016
4	0.44*	11.79±1.11	Blake et al [75]	2012
5	0.51	13.38±0.18	BOSS collaboration [74]	2016
6	0.51	13.62±0.25	DESI Collaboration [72]	2024
7	0.54*	14.76±0.68	Seo et al [76]	2012
8	0.57	14.74±0.24	BOSS collaboration [74]	2016
9	0.59*	15.29±0.25	Chuang et al [73]	2016
10	0.60*	14.99±1.04	Blake et al [75]	2012
11	0.61	15.45±0.22	BOSS collaboration [74]	2016
12	0.70*	17.28±0.89	Sridhar et al [77]	2020
13	0.70	17.96±0.51	Zhao Gong-bo et al [78]	2021
14	0.71	16.85±0.32	DESI Collaboration [72]	2024
15	0.73*	18,03±1.26	Blake et al [75]	2012
16	0.77	18.85±0.38	Wang et al [79]	2020
17	0.80	19.54±2.07	Zhu et al [80]	2018
18	0.85	19.51±0.41	DES collaboration [81]	2024
19	0.85	19.5±1.0	Tamone et al[82], de Mattia et al[83]	2020
20	0.87*	21.39±1.39	Sridhar et al [77]	2020
21	0.93	21.71±0.28	DESI Collaboration [72]	2024
22	1.00	23.13±2.07	Zhu et al [80]	2018
23	1.32	27.79±0.69	DESI Collaboration [72]	2024
24	1.48	30.21±0.79	Hou et al[84], Neveux et al[85]	2020
25	1.50	30.51±1.85	Zhu et al [80]	2018
26	2.00	36.18±1.69	Zhu et al [80]	2018
27	2.20	38.09±1.73	Zhu et al [80]	2018
28	2.33	37.5±1.1	Du Mas des Bourboux et al[86]	2020
29	2.33	39.71±0.94	DESI Collaboration [72]	2024
30	2.34*	37.72±2.18	Delubac et al [87]	2014
31	2.35	36.3±1.8	Blomqvist et al [88]	2019
32	2.40	36.6±1.2	De Mas des Bourboux et al [89]	2017

where we estimate ($D_M^{obs}(z_i)$) using the Planck18 best fit value for $r_d = 147.18 Mpc$. By minimizing this function we obtain the best fit values for h and Ω_{0m} . The parameter uncertainties were again calculated using the Fisher matrix:

$$F_{ij} = \frac{1}{2} \frac{\partial^2 \chi^2(p)}{\partial p_i \partial p_j} \quad (2.21)$$

with the two parameters p_i and p_j being Ω_{0m} and h . The uncertainties in this case are the square roots of the diagonal elements of the inverse Fisher matrix. The corresponding contour plots can then be constructed to represent these results.

III.3. Model Residuals for the w CDM and Λ_s CDM Models

The study of $H(z)$ deformation models is driven by the need for a cosmological framework that is in agreement with Cosmic Microwave Background (CMB) observations at high redshifts ($z \simeq 1100$) as well as with local measurements of the Hubble constant (H_0). These models are designed to maintain the angular diameter distance to the sound horizon scale at recombination as observed by the Planck18/ Λ CDM model, thereby ensuring consistency with the CMB power spectrum. They also assume that $\Omega_{0m}h^2$ has the same value as the one measured by the CMB angular power spectrum while setting constraining h by local measurements [44]. Interesting such models are the w CDM [44] and Λ_s CDM [55, 64] models investigated for their $H(z)$ deformation approach to the H_0 tension.

w CDM Model: The w CDM model modifies the standard equation of state for dark energy, w , from the Planck18/ Λ CDM value of -1 . The Hubble parameter for this model is given by

$$\left(\frac{H}{H_0}\right)^2 = \Omega_{r0}(1+z)^4 + \Omega_{m0}(1+z)^3 + \Omega_{DE0}(1+z)^{3(1+w)}. \quad (2.22)$$

Λ_s CDM Model: Alternatively, the Λ_s CDM model posits a step-like alteration in the dark energy density at a transition redshift z_* . The corresponding Hubble parameter is modeled as

$$\left(\frac{H}{H_0}\right)^2 = \Omega_{r0}(1+z)^4 + \Omega_{m0}(1+z)^3 + \Omega_{\Lambda s0} \text{sgn}(z-z_*), \quad (2.23)$$

where sgn represents the signum function, indicative of the dark energy density change.

In this context, the residual distance modulus, $\Delta\mu(z)$, quantifies the difference between the distance modulus as predicted by a given cosmological model, $\mu_{\text{model}}(z)$, and the distance modulus according to the Planck18 Λ CDM standard model, $\mu_{\text{Planck18}/\Lambda\text{CDM}}(z)$. It is defined as:

$$\Delta\mu(z) = \mu_{\text{model}}(z) - \mu_{\text{Planck18}/\Lambda\text{CDM}}(z). \quad (2.24)$$

where 'model' may correspond eg to w CDM or to Λ_s CDM. This residual is a critical diagnostic tool to assess the viability of models such as w CDM and Λ_s CDM in resolving the H_0 tension, by comparing their predictions with the well-established Λ CDM model as fitted to Planck data and with the intermediate SnIa and BAO data.

For the w CDM model, with $w \simeq -1.2$, there is a successful interpolation between the Cepheid-calibrated low- z SnIa measurements and the CMB-inferred distances to the sound horizon at high- z [44]. This is illustrated in Figure 1, where the residual distance moduli for the w CDM model are compared to those of the Λ_s CDM model, with the BAO and SnIa properly calibrated distance moduli residuals and with the SHOES-Pantheon+ Λ CDM [91] and Planck18/ Λ CDM [4] residual distance moduli (the later has central value at 0 by definition). The best fit Λ_s CDM model [55, 64, 92] with parameter values obtained from [92] (Table I last column) ($z_* = 1.72$), provides a better fit to the more constraining SnIa data at the expense of a worse fit to the BAO data which however have larger uncertainties and thus it leads to a better χ^2 than Λ CDM and other $H(z)$ deformation models like w CDM as shown in Fig. 1. Thus this feature or high z 'break' of $H(z)$ provides an advantage for Λ_s CDM but does not overcome the fundamental problem of the $H(z)$ deformation models which is the generic inconsistency between SnIa and BAO data.

Parameter values of $H(z)$ deformation models: For the w CDM model residual we use the cosmic parameters as calculated by the method described in [44]. For the w parameter we use the following formula:

$$h(w) \simeq -0.3093w + 0.3647 \quad (2.25)$$

where for h we set 0.73 to find $w_{\text{model}} = -1.188$. Then, for the present matter density parameter we use the Planck18/ Λ CDM value

$$\overline{\omega_{0m}} = 0.1430 \pm 0.0011 \quad (2.26)$$

where $\overline{\omega_{0m}} = \Omega_{0m}h^2$ which leads to $\Omega_{0m} = 0.267$ for $H(z)$ deformation models consistent with local measurements of h (eg w CDM).

The luminosity distance modulus for the model is as defined in equation (2.1) and the luminosity distance is as defined in equation (2.2), with the adjustment of using H as defined in equation (2.22).

Similarly, we construct the distance modulus residual for the Λ_s CDM model [93] with best fit parameter values as obtained in [92]. The best fit parameter values we use for the Λ_s CDM model are taken as $z_* = 1.72$, $\Omega_{m,\Lambda_s\text{CDM}} = 0.2646$ and $h_{0,\Lambda_s\text{CDM}} = 0.731$. These are taken from [92], specifically from Table 1 last column.

III. RESULTS: THE HUBBLE TENSION IN REDSHIFT BINS

The focus of our analysis is the level of mismatch of the distance moduli measured using BAO with the corresponding distance moduli measured with SnIa at various redshift bins. This is mainly demonstrated in Fig. 1 which shows the distance moduli residuals with respect to Planck18/ Λ CDM of the following:

- The BAO data of the Table I compilation (blue points). The latest DESI data are the green points shown separately for comparison with earlier points. The full BAO data are binned in wide redshift bins in the right panel.
- The binned Pantheon+ data (red points). These are binned in wide redshift bins in the right panel. The full Pantheon+ distance moduli are also shown in the grey background. The bin corresponding to $z < 0.01$ has a much higher residual distance modulus compared to other bins due to the volumetric redshift scatter bias [68].
- The Planck18/ Λ CDM model with uncertainties (upper band around zero).

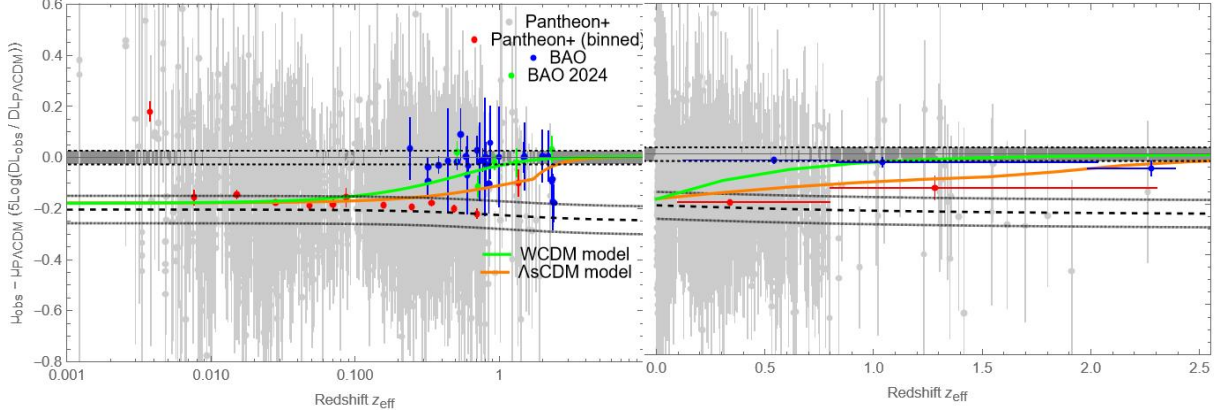


FIG. 1: The binned BAO and Pantheon+ luminosity distance moduli (residuals with respect to the Planck18/ Λ CDM). The residual distance moduli for the best fit w CDM and Λ_s CDM are also shown. Larger redshift bins are shown in the right panel. The inconsistency between BAO and SnIa measured distance moduli is evident. The full Pantheon+ distance moduli are also shown in the grey background. The green points correspond to the latest DESI BAO data.

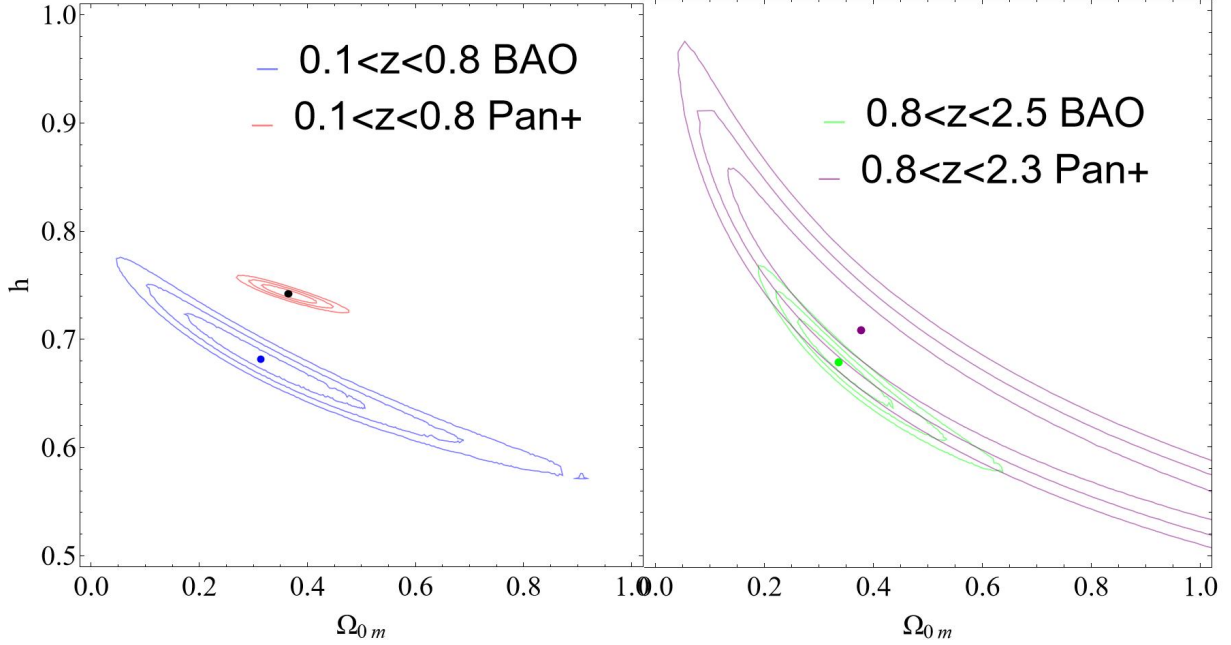


FIG. 2: The consistency between BAO and Pantheon+ data for the low (left) and high (right) redshift bins. Notice that the discrepancy is significantly larger for the low redshift bin.

- The Pantheon+ best fit Λ CDM model (lower band around -0.2).
- The w CDM model designed to interpolate between the SH0ES H_0 and the Planck18 angular diameter distance to recombination consistent with the CMB angular power spectrum data (green line)
- The best fit Λ_s CDM model with respect to Pantheon+, BAO, SH0ES and CMB data with

best fit discussed in the previous section.

The following comments can be made on the results shown in Fig. 1

- There is a clear overall tension between the distance moduli measured by BAO and SnIa data. The distance moduli Planck18/ Λ CDM residuals measured by BAO appear to be systematically higher than the distance moduli residuals measured by SnIa

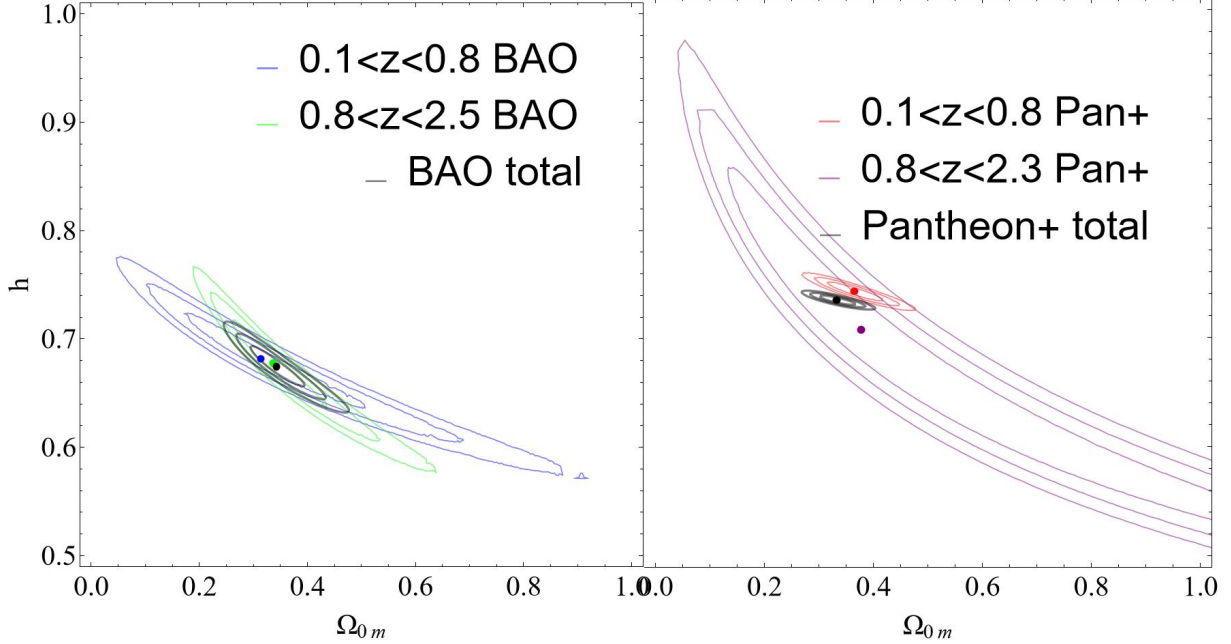


FIG. 3: The consistency between low and high redshift bins for BAO (left) and Pantheon+ (right) data. Notice that there is no evident inconsistency between the redshift bins in the context of each individual dataset.

TABLE II: Best-fit cosmological parameters for two redshift bins within the Λ CDM model.

Redshift Bin	Ω_{0m}	h	M_B
First BAO Bin ($0.1 < z < 0.8$)	0.3 ± 0.1	0.68 ± 0.03	-
Second BAO Bin ($0.8 < z < 2.3$)	0.34 ± 0.06	0.68 ± 0.03	-
First Pan+ Bin ($0.1 < z < 0.8$)	$0.37^{+0.04}_{-0.06}$	$0.742^{+0.008}_{-0.01}$	$-19.21^{+0.02}_{-0.03}$
Second Pan+ Bin ($0.8 < z < 2.3$)	$0.38^{+1}_{-0.2}$	$0.71^{+0.1}_{-0.2}$	$-19.20^{+0.7}_{-0.4}$
Total BAO	0.34 ± 0.03	0.67 ± 0.01	-
Total Pantheon+	0.33 ± 0.02	0.73 ± 0.01	-19.25 ± 0.03

calibrated by Cepheids but lower compared to Planck18/ Λ CDM especially at $z > 1$. Similarly, the model independent binned measured SnIa distance moduli appear to be slightly higher than the expected with respect to the best fit Pantheon+ Λ CDM residual band (the lower stripe in the figure).

- This tension is less significant for redshift $z > 1$ where the SnIa distance moduli residuals with respect to Planck18/ Λ CDM increase while the BAO distance moduli residuals appear to decrease. This reduction of the tension at high z may be viewed as a hint for an $H(z)$ deformation with respect to Planck18/ Λ CDM which however by itself is not sufficient to fully resolve the Hubble tension. This deformation is better expressed by the best fit Λ_s CDM model than by the best fit w CDM model.
- Both $H(z)$ deformation models, w CDM and

Λ_s CDM interpolate successfully between the Planck18/ Λ CDM distance modulus to recombination and the Pantheon+ Λ CDM distance moduli measured by the distance ladder calibrated SnIa at low z . However they can not fit simultaneously the BAO and SnIa distance moduli measured at intermediate redshifts since these are inconsistent with each other.

- The Λ_s CDM model, due to its high z $H(z)$ transition, appears to provide a better fit to the more constraining SnIa data than the more constraining SnIa data than the smooth w CDM best fit model. This seems to explain its overall improved quality of fit to the data compared to other $H(z)$ deformation models that attempt to resolve the Hubble tension.

The consistency level between BAO and Pantheon+ SnIa data in the context of Λ CDM is demon-

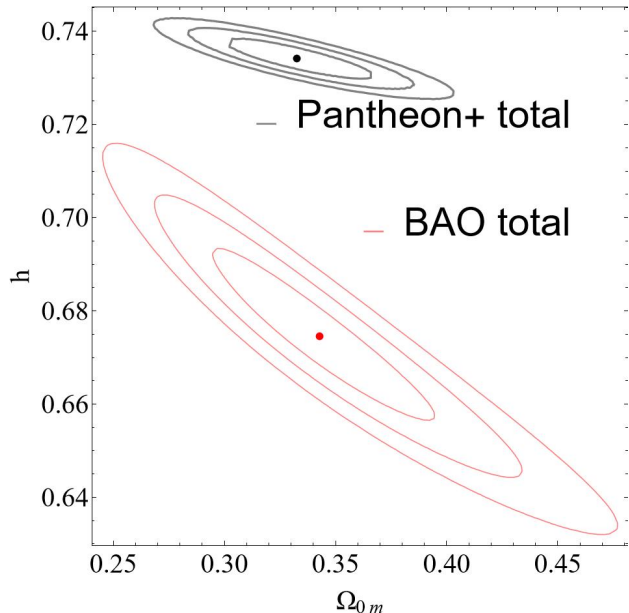


FIG. 4: The likelihood contours of Λ CDM parameters obtained with the full BAO and Pantheon+ samples. The tension between the total BAO and Pantheon+ data sets in intermediate redshifts is apparent.

strated also in Fig. 2. The Λ CDM h - Ω_{0m} likelihood contours are shown for both BAO and SnIa for two large redshift bins $z \in [0.1, 0.8]$ and $z \in [0.8, 2.5]$. Clearly the best fit parameter values are in more than 4σ tension in the low redshift bin while the tension reduces to less than 2σ in the high redshift bin.

The internal consistency between the high and low redshift bins of the BAO and Pantheon+ SnIa samples is tested in Fig. 3 where we show the parameter likelihood contours for the two bins of the BAO-Pantheon+ samples and for full samples. For the BAO sample the two redshift bins are clearly consistent with each other and with the full BAO dataset while for the Pantheon+ sample there is a mild 2σ tension between the low redshift bin and the full sample in the direction of h . This is also shown in the best fit parameter values with uncertainties shown in Table II. Finally, the tension between the full BAO and full Pantheon+ SnIa data is more clearly demonstrated in Fig. 4.

IV. CONCLUSION AND DISCUSSION

We have explored the level of consistency between the distance moduli of an extensive up to date compilation of BAO and the Pantheon+ SnIa data as a

function of redshift. Using a direct comparison of the measured luminosity distance moduli in redshift bins as well as a comparison of the Λ CDM best fit parameter values in low and high z redshift bins we demonstrated the level of tension between the BAO and SnIa at various redshift bins. This discrepancy is mainly due to the well known inconsistency of the calibrators used in each sample (recombination sound horizon vs distance ladder calibration of SnIa with Cepheids) known as the Hubble tension. Since we have used data at intermediate redshifts we were able to identify the redshift dependence of this tension as expressed through BAO and SnIa data. In this context our analysis may be viewed as a redshift tomography of the Hubble tension.

We found that the Hubble tension has more prominent presence in relatively lower redshifts $z \in [0.1, 0.8]$. This effect is not only due to the higher precision of both the BAO and SnIa data in this redshift range. It is also due to a trend of the best fit values of both distance moduli and Λ CDM best fit parameters to become more consistent between BAO and SnIa at higher redshift bins ($z \in [0.8, 2.5]$). This improved consistency between BAO and SnIa data at higher redshift compared to lower redshifts in the context of distance moduli and Λ CDM best fit parameters, may also be interpreted as a high z deformation of $H(z)$ with respect to Λ CDM.

Even though, this deformation can be well expressed by properly designed models like Λ_s CDM, it is clear from our results that it can not by itself provide good fit to all data. This is due to the calibrator induced inconsistency between the BAO and Pantheon+ SnIa data which is more prominent at the redshift range $z \in [0.1, 0.8]$ ².

While there may be correlation among some of the BAO points of our sample, this covariance is in most cases not available in the literature. Thus, by including most available BAO data, we chose to maximize information rather than independence. This approximation may have introduced some bias in our results. Since our sample is not very extensive we estimate that this bias is subdominant and does not change the main features of our results.

Interesting extensions of the present analysis include the consideration of additional data like Cosmic Chronometers or multimessenger standard siren data for the determination of the distance moduli in the redshift range considered, This direct comparison with the measured BAO and SnIa measured

² This inconsistency between BAO and SnIa distance moduli was first pointed out in Ref. [63] using older BAO and SnIa data, even though no redshift tomography was implemented there.

distance moduli could provide hints about the accuracy of the assumed calibrators (sound horizon vs Cepheid based distance ladder)

Numerical analysis files: The Mathematica v13 notebooks and data that lead to the construction of the figures of the paper may be downloaded from [this url](#).

ACKNOWLEDGEMENTS

We thank Adrià Gómez-Valent, Sunny Vagnozzi, Santi Avila and Eoin Colgain for useful comments. This article is based upon work from COST Action CA21136 - Addressing observational tensions in cosmology with systematics and fundamental physics (CosmoVerse), supported by COST (European Cooperation in Science and Technology). This project was also supported by the Hellenic Foundation for Research and Innovation (H.F.R.I.), under the "First call for H.F.R.I. Research Projects to support Faculty members and Researchers and the procurement of high-cost research equipment Grant" (Project Number: 789).

V. APPENDIX

Here we explain the way in which we obtained the D_M/r_d measurements of Table I for the datapoints

with *:

For the measurements 1 and 9, [73] provides the following measurements of $D_A(z) * (r_{s, fid}/r_s)$: $D_A(0.32) * (r_{s, fid}/r_s) = 956 \pm 28 Mpc$ and $D_A(0.59) * (r_{s, fid}/r_s) = 1421 \pm 23 Mpc$. Since $D_M = D_A(z + 1)$, to obtain the $D_M(z)/r_d$ values shown on the table we simply need to multiply by $(r_s/r_{s, fid})$ to obtain the measurement of D_A and then to multiply by $((z + 1)/r_d)$. The fiducial value $r_{s, fid}$ in [73] is $r_{s, fid} = 147.66$ and we use $r_d = 147.18$ and $r_s = 147.09$. We do the same to obtain the uncertainty of the measurement.

For the measurements 4, 10 and 15, [75] provides the following measurements of $D_A(z)$: $D_A(0.44) = 1205 \pm 114 Mpc$, $D_A(0.60) = 1380 \pm 95 Mpc$ and $D_A(0.73) = 1534 \pm 107 Mpc$. To obtain D_M/r_d we simply need to multiply by $((z + 1)/r_d)$. We do the same to obtain the uncertainty of the measurements. [76] (measurement 7) and [87] (measurement 30) also provide measurements of D_A and thus we follow the same steps. [76] provides the following: $D_A(0.54) = 1411 \pm 65 Mpc$. [87] provides the following: $D_A(2.34) = 1662 \pm 96 Mpc$.

For measurements 12 and 20, [77] provides the following: $D_A(0.697) = (1499 \pm 77 Mpc)(r_d/r_{d, fid})$ and $D_A(0.874) = (1680 \pm 109 Mpc)(r_d/r_{d, fid})$. Therefore, to obtain measurements of D_M/r_d we need to multiply the results of D_A by $((z + 1)/r_d)$. We do the same to obtain the uncertainty of the measurement. In [77] the fiducial value of r_d is $r_{d, fid} = 147.21$.

-
- [1] Leandros Perivolaropoulos and Foteini Skara, "Challenges for Λ CDM: An update," *New Astron. Rev.* **95**, 101659 (2022), arXiv:2105.05208 [astro-ph.CO].
 - [2] Elcio Abdalla *et al.*, "Cosmology intertwined: A review of the particle physics, astrophysics, and cosmology associated with the cosmological tensions and anomalies," *JHEAp* **34**, 49–211 (2022), arXiv:2203.06142 [astro-ph.CO].
 - [3] Eleonora Di Valentino, Olga Mena, Supriya Pan, Luca Visinelli, Weiqiang Yang, Alessandro Melchiorri, David F. Mota, Adam G. Riess, and Joseph Silk, "In the realm of the Hubble tension—a review of solutions," *Class. Quant. Grav.* **38**, 153001 (2021), arXiv:2103.01183 [astro-ph.CO].
 - [4] N. Aghanim *et al.* (Planck), "Planck 2018 results. VI. Cosmological parameters," *Astron. Astrophys.* **641**, A6 (2020), [Erratum: *Astron. Astrophys.* 652, C4 (2021)], arXiv:1807.06209 [astro-ph.CO].
 - [5] Valerio Marra and Leandros Perivolaropoulos, "Rapid transition of Geff at $z \simeq 0.01$ as a possible solution of the Hubble and growth tensions," *Phys. Rev. D* **104**, L021303 (2021), arXiv:2102.06012 [astro-ph.CO].
 - [6] George Alestas, Lavrentios Kazantzidis, and Leandros Perivolaropoulos, " $w - M$ phantom transition at $z_t < 0.1$ as a resolution of the Hubble tension," *Phys. Rev. D* **103**, 083517 (2021), arXiv:2012.13932 [astro-ph.CO].
 - [7] Leandros Perivolaropoulos and Foteini Skara, "Hubble tension or a transition of the Cepheid SNIa calibrator parameters?" *Phys. Rev. D* **104**, 123511 (2021), arXiv:2109.04406 [astro-ph.CO].
 - [8] Leandros Perivolaropoulos and Foteini Skara, "Gravitational transitions via the explicitly broken symmetron screening mechanism," *Phys. Rev. D* **106**, 043528 (2022), arXiv:2203.10374 [astro-ph.CO].
 - [9] Leandros Perivolaropoulos and Foteini Skara, "A Reanalysis of the Latest SH0ES Data for H_0 : Effects of New Degrees of Freedom on the Hubble Tension," *Universe* **8**, 502 (2022), arXiv:2208.11169 [astro-ph.CO].
 - [10] George Alestas, Ioannis Antoniou, and Leandros Perivolaropoulos, "Hints for a Gravitational Transition in Tully–Fisher Data," *Universe* **7**, 366 (2021), arXiv:2104.14481 [astro-ph.CO].
 - [11] Vivian Poulin, Tristan L. Smith, Tanvi Karwal, and

- Marc Kamionkowski, “Early Dark Energy Can Resolve The Hubble Tension,” *Phys. Rev. Lett.* **122**, 221301 (2019), arXiv:1811.04083 [astro-ph.CO].
- [12] Marc Kamionkowski and Adam G. Riess, “The Hubble Tension and Early Dark Energy,” *Ann. Rev. Nucl. Part. Sci.* **73**, 153–180 (2023), arXiv:2211.04492 [astro-ph.CO].
- [13] Théo Simon, Pierre Zhang, Vivian Poulin, and Tristan L. Smith, “Updated constraints from the effective field theory analysis of the BOSS power spectrum on early dark energy,” *Phys. Rev. D* **107**, 063505 (2023), arXiv:2208.05930 [astro-ph.CO].
- [14] Matteo Braglia, William T. Emond, Fabio Finelli, A. Emir Gumrukcuoglu, and Kazuya Koyama, “Unified framework for early dark energy from α -attractors,” *Phys. Rev. D* **102**, 083513 (2020), arXiv:2005.14053 [astro-ph.CO].
- [15] Florian Niedermann and Martin S. Sloth, “Resolving the Hubble tension with new early dark energy,” *Phys. Rev. D* **102**, 063527 (2020), arXiv:2006.06686 [astro-ph.CO].
- [16] Tristan L. Smith, Vivian Poulin, José Luis Bernal, Kimberly K. Boddy, Marc Kamionkowski, and Riccardo Murgia, “Early dark energy is not excluded by current large-scale structure data,” *Phys. Rev. D* **103**, 123542 (2021), arXiv:2009.10740 [astro-ph.CO].
- [17] K. Rezazadeh, A. Ashoorioon, and D. Grin, “Cascading Dark Energy,” (2022), arXiv:2208.07631 [astro-ph.CO].
- [18] Matteo Braglia, Mario Ballardini, Fabio Finelli, and Kazuya Koyama, “Early modified gravity in light of the H_0 tension and LSS data,” *Phys. Rev. D* **103**, 043528 (2021), arXiv:2011.12934 [astro-ph.CO].
- [19] Philippe Brax, Carsten van de Bruck, Sebastien Clesse, Anne-Christine Davis, and Gregory Sculthorpe, “Early Modified Gravity: Implications for Cosmology,” *Phys. Rev. D* **89**, 123507 (2014), arXiv:1312.3361 [astro-ph.CO].
- [20] Tal Adi and Ely D. Kovetz, “Can conformally coupled modified gravity solve the Hubble tension?” *Phys. Rev. D* **103**, 023530 (2021), arXiv:2011.13853 [astro-ph.CO].
- [21] Timothy Clifton, Pedro G. Ferreira, Antonio Padilla, and Constantinos Skordis, “Modified Gravity and Cosmology,” *Phys. Rept.* **513**, 1–189 (2012), arXiv:1106.2476 [astro-ph.CO].
- [22] Meng-Xiang Lin, Marco Raveri, and Wayne Hu, “Phenomenology of Modified Gravity at Recombination,” *Phys. Rev. D* **99**, 043514 (2019), arXiv:1810.02333 [astro-ph.CO].
- [23] Eleonora Di Valentino, Alessandro Melchiorri, and Joseph Silk, “Cosmological hints of modified gravity?” *Phys. Rev. D* **93**, 023513 (2016), arXiv:1509.07501 [astro-ph.CO].
- [24] Yashar Akrami *et al.* (CANTATA), *Modified Gravity and Cosmology: An Update by the CANTATA Network*, edited by Emmanuel N. Saridakis, Ruth Lazkoz, Vincenzo Salzano, Paulo Vargas Moniz, Salvatore Capozziello, Jose Beltrán Jiménez, Mariaferlia De Laurentis, and Gonzalo J. Olmo (Springer, 2021) arXiv:2105.12582 [gr-qc].
- [25] Massimo Rossi, Mario Ballardini, Matteo Braglia, Fabio Finelli, Daniela Paoletti, Alexei A. Starobinsky, and Caterina Umiltà, “Cosmological constraints on post-Newtonian parameters in effectively massless scalar-tensor theories of gravity,” *Phys. Rev. D* **100**, 103524 (2019), arXiv:1906.10218 [astro-ph.CO].
- [26] Matteo Braglia, Mario Ballardini, William T. Emond, Fabio Finelli, A. Emir Gumrukcuoglu, Kazuya Koyama, and Daniela Paoletti, “Larger value for H_0 by an evolving gravitational constant,” *Phys. Rev. D* **102**, 023529 (2020), arXiv:2004.11161 [astro-ph.CO].
- [27] Guillermo Franco Abellán, Matteo Braglia, Mario Ballardini, Fabio Finelli, and Vivian Poulin, “Probing early modification of gravity with Planck, ACT and SPT,” *JCAP* **12**, 017 (2023), arXiv:2308.12345 [astro-ph.CO].
- [28] Osamu Seto and Yo Toda, “Comparing early dark energy and extra radiation solutions to the Hubble tension with BBN,” *Phys. Rev. D* **103**, 123501 (2021), arXiv:2101.03740 [astro-ph.CO].
- [29] Jeremy Sakstein and Mark Trodden, “Early Dark Energy from Massive Neutrinos as a Natural Resolution of the Hubble Tension,” *Phys. Rev. Lett.* **124**, 161301 (2020), arXiv:1911.11760 [astro-ph.CO].
- [30] Sunny Vagnozzi, “New physics in light of the H_0 tension: An alternative view,” *Phys. Rev. D* **102**, 023518 (2020), arXiv:1907.07569 [astro-ph.CO].
- [31] George Alestas and Leandros Perivolaropoulos, “Late-time approaches to the Hubble tension deforming $H(z)$, worsen the growth tension,” *Mon. Not. Roy. Astron. Soc.* **504**, 3956–3962 (2021), arXiv:2103.04045 [astro-ph.CO].
- [32] Karsten Jedamzik, Levon Pogosian, and Gong-Bo Zhao, “Why reducing the cosmic sound horizon alone can not fully resolve the Hubble tension,” *Commun. in Phys.* **4**, 123 (2021), arXiv:2010.04158 [astro-ph.CO].
- [33] Sunny Vagnozzi, “Seven Hints That Early-Time New Physics Alone Is Not Sufficient to Solve the Hubble Tension,” *Universe* **9**, 393 (2023), arXiv:2308.16628 [astro-ph.CO].
- [34] Sunny Vagnozzi, “Consistency tests of Λ CDM from the early integrated Sachs-Wolfe effect: Implications for early-time new physics and the Hubble tension,” *Phys. Rev. D* **104**, 063524 (2021), arXiv:2105.10425 [astro-ph.CO].
- [35] Xiaolei Li and Arman Shafieloo, “A Simple Phenomenological Emergent Dark Energy Model can Resolve the Hubble Tension,” *Astrophys. J. Lett.* **883**, L3 (2019), arXiv:1906.08275 [astro-ph.CO].
- [36] Supriya Pan, Weiqiang Yang, Eleonora Di Valentino, Arman Shafieloo, and Subenoy Chakraborty, “Reconciling H_0 tension in a six parameter space?” *JCAP* **06**, 062 (2020), arXiv:1907.12551 [astro-ph.CO].
- [37] Sirachak Panpanich, Piyabut Burikham, Supakchai Ponglertsakul, and Lunchakorn Tannukij, “Re-

- solving Hubble Tension with Quintom Dark Energy Model,” *Chin. Phys. C* **45**, 015108 (2021), arXiv:1908.03324 [gr-qc].
- [38] Eleonora Di Valentino, Alessandro Melchiorri, Olga Mena, and Sunny Vagnozzi, “Interacting dark energy in the early 2020s: A promising solution to the H_0 and cosmic shear tensions,” *Phys. Dark Univ.* **30**, 100666 (2020), arXiv:1908.04281 [astro-ph.CO].
- [39] Eleonora Di Valentino, Alessandro Melchiorri, Olga Mena, and Sunny Vagnozzi, “Nonminimal dark sector physics and cosmological tensions,” *Phys. Rev. D* **101**, 063502 (2020), arXiv:1910.09853 [astro-ph.CO].
- [40] Xiaolei Li and Arman Shafieloo, “Evidence for Emergent Dark Energy,” *Astrophys. J.* **902**, 58 (2020), arXiv:2001.05103 [astro-ph.CO].
- [41] Steven J. Clark, Kyriakos Vattis, and Savvas M. Koushiappas, “Cosmological constraints on late-universe decaying dark matter as a solution to the H_0 tension,” *Phys. Rev. D* **103**, 043014 (2021), arXiv:2006.03678 [astro-ph.CO].
- [42] Eleonora Di Valentino, Eric V. Linder, and Alessandro Melchiorri, “ H_0 ex machina: Vacuum metamorphosis and beyond H_0 ,” *Phys. Dark Univ.* **30**, 100733 (2020), arXiv:2006.16291 [astro-ph.CO].
- [43] George Alestas, David Camarena, Eleonora Di Valentino, Lavrentios Kazantzidis, Valerio Marra, Savvas Nesseris, and Leandros Perivolaropoulos, “Late-transition versus smooth $H(z)$ -deformation models for the resolution of the Hubble crisis,” *Phys. Rev. D* **105**, 063538 (2022), arXiv:2110.04336 [astro-ph.CO].
- [44] G. Alestas, L. Kazantzidis, and L. Perivolaropoulos, “ H_0 tension, phantom dark energy, and cosmological parameter degeneracies,” *Phys. Rev. D* **101**, 123516 (2020), arXiv:2004.08363 [astro-ph.CO].
- [45] Samuel Brieden, Héctor Gil-Marín, and Licia Verde, “Model-agnostic interpretation of 10 billion years of cosmic evolution traced by BOSS and eBOSS data,” *JCAP* **08**, 024 (2022), arXiv:2204.11868 [astro-ph.CO].
- [46] Ryan E. Keeley and Arman Shafieloo, “Ruling Out New Physics at Low Redshift as a Solution to the H_0 Tension,” *Phys. Rev. Lett.* **131**, 111002 (2023), arXiv:2206.08440 [astro-ph.CO].
- [47] A. Chen *et al.* (DES), “Constraints on dark matter to dark radiation conversion in the late universe with DES-Y1 and external data,” *Phys. Rev. D* **103**, 123528 (2021), arXiv:2011.04606 [astro-ph.CO].
- [48] Luis A. Anchordoqui, Vernon Barger, Danny Marfatia, and Jorge F. Soriano, “Decay of multiple dark matter particles to dark radiation in different epochs does not alleviate the Hubble tension,” *Phys. Rev. D* **105**, 103512 (2022), arXiv:2203.04818 [astro-ph.CO].
- [49] S. Mau *et al.* (DES), “Milky Way Satellite Census. IV. Constraints on Decaying Dark Matter from Observations of Milky Way Satellite Galaxies,” *Astrophys. J.* **932**, 128 (2022), arXiv:2201.11740 [astro-ph.CO].
- [50] Rong-Gen Cai, Zong-Kuan Guo, Shao-Jiang Wang, Wang-Wei Yu, and Yong Zhou, “No-go guide for late-time solutions to the Hubble tension: Matter perturbations,” *Phys. Rev. D* **106**, 063519 (2022), arXiv:2202.12214 [astro-ph.CO].
- [51] Lavinia Heisenberg, Hector Villarrubia-Rojo, and Jann Zosso, “Can late-time extensions solve the H_0 and σ_8 tensions?” *Phys. Rev. D* **106**, 043503 (2022), arXiv:2202.01202 [astro-ph.CO].
- [52] Sunny Vagnozzi, Fabio Pacucci, and Abraham Loeb, “Implications for the Hubble tension from the ages of the oldest astrophysical objects,” *JHEAp* **36**, 27–35 (2022), arXiv:2105.10421 [astro-ph.CO].
- [53] Zahra Davari and Nima Khosravi, “Can decaying dark matter scenarios alleviate both H_0 and σ_8 tensions?” *Mon. Not. Roy. Astron. Soc.* **516**, 4373–4382 (2022), arXiv:2203.09439 [astro-ph.CO].
- [54] Adrià Gómez-Valent, Arianna Favale, Marina Migliaccio, and Anjan A. Sen, “Late-time phenomenology required to solve the H_0 tension in view of the cosmic ladders and the anisotropic and angular BAO datasets,” *Phys. Rev. D* **109**, 023525 (2024), arXiv:2309.07795 [astro-ph.CO].
- [55] Ozgur Akarsu, Suresh Kumar, Emre Özüiker, J. Alberto Vazquez, and Anita Yadav, “Relaxing cosmological tensions with a sign switching cosmological constant: Improved results with Planck, BAO, and Pantheon data,” *Phys. Rev. D* **108**, 023513 (2023), arXiv:2211.05742 [astro-ph.CO].
- [56] Adam G. Riess *et al.*, “A Comprehensive Measurement of the Local Value of the Hubble Constant,” *Astrophys. J. Lett.* **934**, L7 (2022), arXiv:2112.04510 [astro-ph.CO].
- [57] Maria Giovanna Dainotti, Biagio De Simone, Tiziano Schiavone, Giovanni Montani, Enrico Rinaldi, and Gaetano Lambiase, “On the Hubble constant tension in the SNe Ia Pantheon sample,” *Astrophys. J.* **912**, 150 (2021), arXiv:2103.02117 [astro-ph.CO].
- [58] Eoin Ó. Colgáin, M. M. Sheikh-Jabbari, Rance Solomon, Giada Bargiacchi, Salvatore Capozziello, Maria Giovanna Dainotti, and Dejan Stojkovic, “Revealing intrinsic flat Λ CDM biases with standardizable candles,” *Phys. Rev. D* **106**, L041301 (2022), arXiv:2203.10558 [astro-ph.CO].
- [59] Chethan Krishnan, Roya Mohayaee, Eoin Ó. Colgáin, M. M. Sheikh-Jabbari, and Lu Yin, “Does Hubble tension signal a breakdown in FLRW cosmology?” *Class. Quant. Grav.* **38**, 184001 (2021), arXiv:2105.09790 [astro-ph.CO].
- [60] X. D. Jia, J. P. Hu, and F. Y. Wang, “Evidence of a decreasing trend for the Hubble constant,” *Astron. Astrophys.* **674**, A45 (2023), arXiv:2212.00238 [astro-ph.CO].
- [61] C. Krishnan, Eoin Ó. Colgáin, Ruchika, Anjan A. Sen, M. M. Sheikh-Jabbari, and Tao Yang, “Is there an early Universe solution to Hubble tension?” *Phys. Rev. D* **102**, 103525 (2020), arXiv:2002.06044 [astro-ph.CO].
- [62] C. Krishnan, E. Ó. Colgáin, M. M. Sheikh-Jabbari, and Tao Yang, “Running Hubble Tension and a H_0 Diagnostic,” *Phys. Rev. D* **103**, 103509 (2021),

- arXiv:2011.02858 [astro-ph.CO].
- [63] Levon Pogossian, Marco Raveri, Kazuya Koyama, Matteo Martinelli, Alessandra Silvestri, Gong-Bo Zhao, Jian Li, Simone Peirone, and Alex Zucca, “Imprints of cosmological tensions in reconstructed gravity,” *Nature Astron.* **6**, 1484–1490 (2022), arXiv:2107.12992 [astro-ph.CO].
- [64] Özgür Akarsu, John D. Barrow, Luis A. Escamilla, and J. Alberto Vazquez, “Graduated dark energy: Observational hints of a spontaneous sign switch in the cosmological constant,” *Phys. Rev. D* **101**, 063528 (2020), arXiv:1912.08751 [astro-ph.CO].
- [65] D. Brout *et al.* (DES), “First Cosmology Results Using Type Ia Supernovae From the Dark Energy Survey: Analysis, Systematic Uncertainties, and Validation,” *Astrophys. J.* **874**, 150 (2019), arXiv:1811.02377 [astro-ph.CO].
- [66] Isaac Tutusaus, Brahim Lamine, and Alain Blanchard, “Model-independent cosmic acceleration and redshift-dependent intrinsic luminosity in type-Ia supernovae,” *Astron. Astrophys.* **625**, A15 (2019), arXiv:1803.06197 [astro-ph.CO].
- [67] Karsten Jedamzik and Levon Pogossian, “Relieving the Hubble tension with primordial magnetic fields,” *Phys. Rev. Lett.* **125**, 181302 (2020), arXiv:2004.09487 [astro-ph.CO].
- [68] Leandros Perivolaropoulos and Foteini Skara, “On the homogeneity of SnIa absolute magnitude in the Pantheon+ sample,” *Mon. Not. Roy. Astron. Soc.* **520**, 5110–5125 (2023), arXiv:2301.01024 [astro-ph.CO].
- [69] Éric Aubourg *et al.* (BOSS), “Cosmological implications of baryon acoustic oscillation measurements,” *Phys. Rev. D* **92**, 123516 (2015), arXiv:1411.1074 [astro-ph.CO].
- [70] Dillon Brout *et al.*, “The Pantheon+ Analysis: SuperCal-fragilistic Cross Calibration, Retrained SALT2 Light-curve Model, and Calibration Systematic Uncertainty,” *Astrophys. J.* **938**, 111 (2022), arXiv:2112.03864 [astro-ph.CO].
- [71] Dan Scolnic *et al.*, “The Pantheon+ Analysis: The Full Data Set and Light-curve Release,” *Astrophys. J.* **938**, 113 (2022), arXiv:2112.03863 [astro-ph.CO].
- [72] A. G. Adame *et al.* (DESI), “DESI 2024 VI: Cosmological Constraints from the Measurements of Baryon Acoustic Oscillations,” (2024), arXiv:2404.03002 [astro-ph.CO].
- [73] Chia-Hsun Chuang *et al.* (BOSS), “The clustering of galaxies in the completed SDSS-III Baryon Oscillation Spectroscopic Survey: single-probe measurements from DR12 galaxy clustering – towards an accurate model,” *Mon. Not. Roy. Astron. Soc.* **471**, 2370–2390 (2017), arXiv:1607.03151 [astro-ph.CO].
- [74] Shadab Alam *et al.* (BOSS), “The clustering of galaxies in the completed SDSS-III Baryon Oscillation Spectroscopic Survey: cosmological analysis of the DR12 galaxy sample,” *Mon. Not. Roy. Astron. Soc.* **470**, 2617–2652 (2017), arXiv:1607.03155 [astro-ph.CO].
- [75] Blake, “The wigglez dark energy survey: Joint measurements of the expansion and growth history at $z \lesssim 1$,” *Monthly Notices of the Royal Astronomical Society* **425**, 405–414 (2012).
- [76] Seo, “Acoustic scale from the angular power spectra of sdss-iii dr8 photometric luminous galaxies,” *The Astrophysical Journal* **761**, 13 (2012).
- [77] Srivatsan Sridhar, Yong-Seon Song, Ashley J. Ross, Rongpu Zhou, Jeffrey A. Newman, Chia-Hsun Chuang, Francisco Prada, Robert Blum, Enrique Gaztañaga, and Martin Landriau, “Clustering of LRGs in the DECaLS DR8 Footprint: Distance Constraints from Baryon Acoustic Oscillations Using Photometric Redshifts,” *Astrophys. J.* **904**, 69 (2020), arXiv:2005.13126 [astro-ph.CO].
- [78] Gong-Bo Zhao *et al.* (eBOSS), “The completed SDSS-IV extended Baryon Oscillation Spectroscopic Survey: a multitracer analysis in Fourier space for measuring the cosmic structure growth and expansion rate,” *Mon. Not. Roy. Astron. Soc.* **504**, 33–52 (2021), arXiv:2007.09011 [astro-ph.CO].
- [79] Yuting Wang *et al.* (eBOSS), “The clustering of the SDSS-IV extended Baryon Oscillation Spectroscopic Survey DR16 luminous red galaxy and emission line galaxy samples: cosmic distance and structure growth measurements using multiple tracers in configuration space,” *Mon. Not. Roy. Astron. Soc.* **498**, 3470–3483 (2020), arXiv:2007.09010 [astro-ph.CO].
- [80] Fangzhou Zhu *et al.* (eBOSS), “The clustering of the SDSS-IV extended Baryon Oscillation Spectroscopic Survey DR14 quasar sample: measuring the anisotropic baryon acoustic oscillations with redshift weights,” *Mon. Not. Roy. Astron. Soc.* **480**, 1096–1105 (2018), arXiv:1801.03038 [astro-ph.CO].
- [81] T. M. C. Abbott *et al.* (DES), “Dark Energy Survey: A 2.1% Measurement of the Angular Baryonic Acoustic Oscillation Scale at Redshift $z_{\text{eff}}=0.85$ from the Final Dataset,” (2024), arXiv:2402.10696 [astro-ph.CO].
- [82] Amélie Tamone *et al.* (eBOSS), “The Completed SDSS-IV extended Baryon Oscillation Spectroscopic Survey: Growth rate of structure measurement from anisotropic clustering analysis in configuration space between redshift 0.6 and 1.1 for the Emission Line Galaxy sample,” *Mon. Not. Roy. Astron. Soc.* **499**, 5527–5546 (2020), arXiv:2007.09009 [astro-ph.CO].
- [83] Arnaud de Mattia *et al.* (eBOSS), “The Completed SDSS-IV extended Baryon Oscillation Spectroscopic Survey: measurement of the BAO and growth rate of structure of the emission line galaxy sample from the anisotropic power spectrum between redshift 0.6 and 1.1,” *Mon. Not. Roy. Astron. Soc.* **501**, 5616–5645 (2021), arXiv:2007.09008 [astro-ph.CO].
- [84] Jiamin Hou *et al.* (eBOSS), “The Completed SDSS-IV extended Baryon Oscillation Spectroscopic Survey: BAO and RSD measurements from anisotropic clustering analysis of the Quasar Sample in configuration space between redshift 0.8 and 2.2,” *Mon. Not. Roy. Astron. Soc.* **500**, 1201–1221 (2020), arXiv:2007.08998 [astro-ph.CO].

- [85] Richard Neveux *et al.* (eBOSS), “The completed SDSS-IV extended Baryon Oscillation Spectroscopic Survey: BAO and RSD measurements from the anisotropic power spectrum of the quasar sample between redshift 0.8 and 2.2,” *Mon. Not. Roy. Astron. Soc.* **499**, 210–229 (2020), arXiv:2007.08999 [astro-ph.CO].
- [86] Héliou du Mas des Bourboux *et al.* (eBOSS), “The Completed SDSS-IV Extended Baryon Oscillation Spectroscopic Survey: Baryon Acoustic Oscillations with Ly α Forests,” *Astrophys. J.* **901**, 153 (2020), arXiv:2007.08995 [astro-ph.CO].
- [87] Timothée Delubac *et al.* (BOSS), “Baryon acoustic oscillations in the Ly α forest of BOSS DR11 quasars,” *Astron. Astrophys.* **574**, A59 (2015), arXiv:1404.1801 [astro-ph.CO].
- [88] Michael Blomqvist *et al.* (eBOSS), “Baryon acoustic oscillations from the cross-correlation of Ly α absorption and quasars in eBOSS DR14,” *Astron. Astrophys.* **629**, A86 (2019), arXiv:1904.03430 [astro-ph.CO].
- [89] Héliou du Mas des Bourboux *et al.* (BOSS), “Baryon acoustic oscillations from the complete SDSS-III Ly α -quasar cross-correlation function at $z = 2.4$,” *Astron. Astrophys.* **608**, A130 (2017), arXiv:1708.02225 [astro-ph.CO].
- [90] William H. Press, Saul A. Teukolsky, William T. Vetterling, and Brian P. Flannery, *Numerical Recipes 3rd Edition: The Art of Scientific Computing* (Cambridge University Press, New York, NY, USA, 2007).
- [91] Dillon Brout *et al.*, “The Pantheon+ Analysis: Cosmological Constraints,” *Astrophys. J.* **938**, 110 (2022), arXiv:2202.04077 [astro-ph.CO].
- [92] Ozgur Akarsu, Eleonora Di Valentino, Suresh Kumar, Rafael C. Nunes, J. Alberto Vazquez, and Anita Yadav, “ Λ_s CDM model: A promising scenario for alleviation of cosmological tensions,” (2023), arXiv:2307.10899 [astro-ph.CO].
- [93] Özgür Akarsu, Suresh Kumar, Emre Özüiker, and J. Alberto Vazquez, “Relaxing cosmological tensions with a sign switching cosmological constant,” *Phys. Rev. D* **104**, 123512 (2021), arXiv:2108.09239 [astro-ph.CO].